Modeling the orientational and positional behavior of polyhedral nanoparticles at fluid-fluid interfaces

U. Gupta, T. Hanrath, and F. A. Escobedo*
School of Chemical and Biomolecular Engineering, Cornell University, Ithaca, New York 14853, USA
(Received 12 August 2017; published 27 October 2017)

Using molecular dynamics simulations to explicitly model fluid molecules, we study the effect of solvent wetting on the behavior of polyhedral nanoparticles at a fluid-fluid interface. First, we quantify the positional and orientational free-energy characteristics of an isolated nanoparticle. Our results suggest that the structure of the interface can introduce nontrivial effects on the preferential particle orientations. A continuum model is proposed to account for the finite-interfacial mixing region, and a qualitative comparison with the molecular simulation results is presented. We examine the effect on the free energy of the system of changes in the particle's solvation preference towards one fluid, and the degree of miscibility between the two fluids. By tuning these interaction parameters, we can potentially access and favor different orientations for the particle shapes examined. Further, we extend the insights gained from single-particle behavior to the attachment of two particles. Our results reveal conditions that could drive the assembly of cuboctahedra into either two-dimensional puckered honeycomb lattices or linear rodlike structures.

DOI: 10.1103/PhysRevMaterials.1.055602

I. INTRODUCTION

Recent advances in the synthesis of colloidal nanoparticles (NPs, aka quantum dots) with precisely controlled size, shape, and composition have introduced a new paradigm of material synthesis. Using NPs as fundamental building blocks of superstructure introduces the ability to control interactions between the particles and thereby tailor the material's properties. Among the various self-assembly strategies that have been reported, interfacial assembly has emerged as the most promising and versatile. By restricting the motion of the NPs to two dimensions, e.g., by depositing them on a flat solid substrate or by pinning them at a fluid-fluid interface, a variety of superlattice structures can be realized from the same building blocks. Numerous experimental efforts [1–5] have been made over the years to increase the repeatability, precision, and control over the self-assembly of colloidal NPs into quasi-two-dimensional (2D) superstructures with programmable symmetry. These quasi-2D superstructures provide important test-beds for the study of fundamental structure-property relations and have found multiple technologically important applications, e.g., in optics [6–8], photovoltaics [9–11], and catalysis [12,13].

The self-assembly of NPs at a fluid-fluid interface is driven by a complex interplay of entropic and enthalpic forces. Although simulation studies have mostly focused on investigating systems dominated by entropic effects through Monte Carlo simulations of hard-core particles [14–17], a few studies have also examined systems exhibiting enthalpic interactions using molecular dynamics (MD) simulations [18,19]. The current work primarily aims to assess the role of enthalpic interactions on the self-assembly process, using a coarse-grained model for the polyhedral NPs and explicit molecules to describe the fluids. The use of polybead models to represent polyhedral objects facilitates not only the implementation of enthalpic interactions but also the use of MD simulations which conveniently exploit multiprocessor computing capabilities.

It has been long known that colloidal NPs possess a strong affinity towards fluid-fluid interfaces and can bind to them irreversibly [20,21]. It is widely believed that the driving force behind this irreversible adsorption is the reduction in the interfacial energy due to contact between the two immiscible fluids. Based on this principle, many analytical models [2–4,22–25] have been developed to capture the orientational behavior of isolated NPs at sharp (zero thickness) interfaces.

In the case of polyhedral particles, understanding and controlling the orientation of the NP relative to the normal of the interface presents an interesting challenge. The NP orientation is typically denoted by the Miller index vector or the NP facet parallel to the plane of the interface. Cilliers and co-workers [26,27] have reported a model for the investigation of the orientation of isolated, nonspherical, micrometer-sized particles at fluid interfaces. Their continuum model showed that cubic particles with a fixed surface energy preferred the $\{100\}$ facet up orientation at low contact angles and the corner-up $\{111\}$ facet up orientation at high contact angles. Evers *et al.* [2] predicted that the most preferred orientation of a cubic NP at a nondeformable, sharp interface is $\{110\}$ facet up. Recent experiments [28,29] have demonstrated that, under certain conditions, cubic NPs at a fluid-fluid interface orient with the $\{111\}$ facet up. Subsequently, by including the effect of capillary deformation in a sharp-interface model, Soligno *et al.* [25] showed that the $\{111\}$ facet up preference of the cube could be captured correctly. Whereas the sharp-interface models may be suitable for applications to relatively larger NPs, the effect of an interfacial region with a finite "thickness" cannot be neglected when the NP size is comparable to the thickness of the interface.

In this work, we seek to establish the underlying thermodynamic principles governing the self-assembly of NPs using flat (fluid) interfaces as templates. The first step in this process is to investigate the behavior of an isolated NP at the interface. For this purpose, we employ solvent-explicit MD simulations to describe the multibody effect of the fluid molecules on the NP. By explicitly modeling the interface, the effect of solvent wetting characteristics on the NP behavior can be

*Corresponding author: fe13@cornell.edu

 ©2017 American Physical Society

more accurately captured. We use these simulations to map out the free energy of the NPs as a function of their orientations and vertical positions with respect to the interface, and thus to identify the preferred NP configurations. We use selected molecular simulation results for a cube shape to illustrate the basis of the general characteristics displayed by an isolated NP at the interface, and to motivate the development of a continuum model where a nondeformable interfacial region of finite thickness contributes explicitly to the free energy of the system.

The rest of this manuscript is organized as follows. In Sec. II, we describe the coarse-grained simulation model and simulation methodology. In Sec. III, we summarize the basis of our continuum model (providing additional details in the Supplemental Material (SM) [30]). In Sec. IV, we present the main results for a single NP near an interface, comparing key simulation data and trends to those predicted by the continuum model. In that section, we also extend the principles developed for a single NP to explain the assembly of two-NP systems, simulating polybead cuboctahedra as a test-bed. Finally, we close with some concluding remarks and an outline of suggested future work in Sec. V.

II. MODELS AND METHODS

A. Coarse-grained model and molecular dynamics (MD)

The base system consists of a single colloidal NP (Fig. 1), suspended at the interface of two vertically stacked immiscible fluids (two NPs are simulated in select cases). For simplicity, the direction perpendicular to the average orientation of the interface is, henceforth, referred to as the vertical direction (represented by the y axis). By construction, the interface is initially located at the center of the simulation box. The interface location is maintained near the box center by adding reflective walls at the box edges perpendicular to the vertical direction. Periodic boundary conditions (PBCs) are imposed in the x and z directions.

The NPs are described using a *polybead model* [31]. The desired shape is carved out from a cubic-close-packed lattice, wherein each face is represented by a well-defined crystallographic plane. The NP is then shaped by placing Lennard-Jones (LJ) beads at the surface or outermost lattice sites only. The surrounding liquids (top solvent and bottom subphase) are explicitly defined as dimers of LJ beads. While such dimers are intended to be a coarse-grained representation of the fluid molecules, they are able to capture the multibody forces associated with the wetting characteristics of NPs and the varying fluid properties across the fluid-fluid interface. Typically, the number of solvent molecules was around 5500.

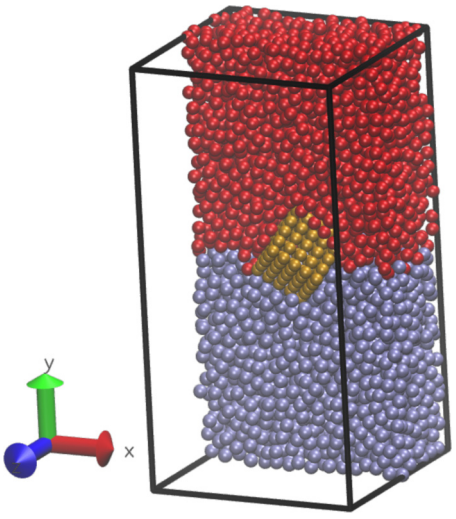

FIG. 1. Snapshot of the polybead model depicting two fluid phases (in red and blue) and a cubic NP (in yellow) at their interface. For the sake of visibility, fluid molecules have been removed from the front half of the simulation box.

The interaction between any two species is modeled by tuning the interactions between their corresponding beads. This inter-bead interaction is defined by the (12-6) cut and linearly shifted Lennard-Jones potential,

$$U(r_{ij}) = \phi(r_{ij}) - \phi(r_c) - (r_{ij} - r_c)\left.\frac{d\phi}{dr_{ij}}\right|_{r_{ij}=r_c}; \quad r_{ij} < r_c, \tag{1}$$

$$\phi(r_{ij}) = 4\varepsilon_{ij}\left[\left(\frac{\sigma}{r_{ij}}\right)^{12} - \left(\frac{\sigma}{r_{ij}}\right)^{6}\right], \tag{2}$$

where r_{ij} is the distance between beads i and j and the cutoff radius is $r_c = 2.5$. The effective diameter (σ) of all beads (in the NP and the two liquids) is taken to be the same ($\sigma = 1.0$). The bond in a liquid dimer is described by the FENE (Finitely Extensible Nonlinear Elastic) potential,

$$U(r) = -0.5 K R_0^2 \ln\left[1 - \left(\frac{r}{R_0}\right)^2\right] + 4\varepsilon\left[\left(\frac{\sigma}{r}\right)^{12} - \left(\frac{\sigma}{r}\right)^{6}\right] + \varepsilon, \tag{3}$$

and the bond length is maintained at 1σ ($K = 30\varepsilon/\sigma^2$, $R_0 = 1.5\sigma$). MD simulations are performed using the canonical (NVT) ensemble in LAMMPS [32]. The simulation temperature is maintained at $0.85\varepsilon/k_B$ using the Nosé-Hoover thermostat. In this work, we only consider systems with a liquid-liquid interface, and so the density is kept close to 0.8 beads/σ^3, and the integration step is 0.005τ. For a single-NP system, the typical simulation box size is $20 \times 40 \times 20\sigma^3$ (in the X-Y-Z dimensions, respectively). Characteristic values of the reduced parameters for comparison with experimental data, as reported in Ref. [33], are $\sigma = 0.4$ nm, $\varepsilon = 100k_B$, and $\tau = 2$ ps.

Using the method given by Savoy and Escobedo [34], the LJ well depth parameter (ε_{ij}) between the NP surface and the fluid is tuned to correspond to a physically relevant contact angle value (θ_{ij}) and the resulting calibration curve is given in the SM (Fig. S1 [30]). The degree of miscibility between the two fluids is determined by the value of $\varepsilon_{S1,S2}$. In the following sections, we first establish a "base case" where the ε_{ij} value between all species is set to 0.5. This ensures that the NP interacts symmetrically with both the fluids, and the respective contact angle values are close to 90°. We subsequently change the interaction parameters to be asymmetric so that the NP is preferentially wetted by a particular fluid, and assess the effect of this asymmetry by comparison with the results from the base case.

B. Free energy (FE) and key degrees of freedom

The microstate of a single NP (and the free energy associated with it) is fully determined by its position and orientation relative to the fluid-fluid interface. We use a vertical position (H) and Euler angles (θ, ψ) to describe such degrees of freedom.

The interface diving surface is defined as the plane parallel to the average orientation of the interface and dividing the finite interface symmetrically through the middle. The distance H from the NP center of mass to the interface-dividing plane is referred to as "vertical" position and is given in reduced units "y/e" where e is the edge length or a characteristic size parameter of the NP. To quantitatively characterize the thermodynamic driving force that controls the vertical position (H) of the NP, we perform umbrella sampling (US) [35] simulations to estimate the underlying free-energy (FE) profile. For this purpose, we divide the vertical position space into overlapping windows and use a harmonic biasing potential to constrain the NP to each window. A weighted histogram analysis method (WHAM) [36] scheme is then used to combine the results from individual simulation windows into the final unbiased FE profile.

NP orientation is represented using the intrinsic Euler angle convention (y-z'-y'') with three angles (ϕ, θ, ψ). The elemental rotations occur about the axes of the local coordinate system (fixed to the NP). Angle ϕ gives the rotation about the y axis, i.e., the axis perpendicular to the interface. Rotation about this axis does not change the NP configuration with respect to the interface, and hence we ignore it. The tilt angle θ describes the rotation about the new (rotated in step 1) z axis, and the spin angle ψ gives the rotation about the new (rotated in step 2) y axis.

For an isolated NP (of a given shape and size) at the interface, a free-energy landscape can be generated with tilt (θ) and spin (ψ) angles as parameters using an US technique. The vertical position of the NP is decoupled from such calculation by allowing it to freely fluctuate around its equilibrium position. The 2D orientation phase space is divided into overlapping windows. Independent MD simulations are run for each window with two discrete harmonic torsion springs constraining the corresponding orientation angles (details in the SM, Sec. 4 [30]). The windows are then stitched together using WHAM to generate the unbiased FE landscape. The global minimum in this landscape helps to identify the preferred orientation of the NP.

III. INTERFACIAL STRUCTURE AND CONTINUUM MODEL

First, we used our MD simulations to probe the presence of hexapolar capillary deformations in the interface for a cubic NP in the $\{111\}$ facet up orientation as predicted by Soligno *et al.* [25]. To do this, the simulation box is set up as described in Sec. II A and a cubic NP is fixed at the origin in the $\{111\}$ facet up orientation. The value of all ε_{ij} is set to 0.5. The box is then divided into three-dimensional (3D) voxels, and the density of the bottom solvent beads, ρ_{S2}, for each voxel is calculated and averaged over time. We simulate two NP sizes, 5σ and 10σ, and the density profiles at various vertical heights are shown in Fig. 2. The approximate heights of capillary deformations for cubic NPs of sizes 5σ and 10σ are estimated (in the SM, Fig. S3 [30]) to be 0.25σ ($0.05e$) and 1.25σ ($0.125e$), respectively. Clearly, as the NP size increases, the capillary deformations become more pronounced and are expected to

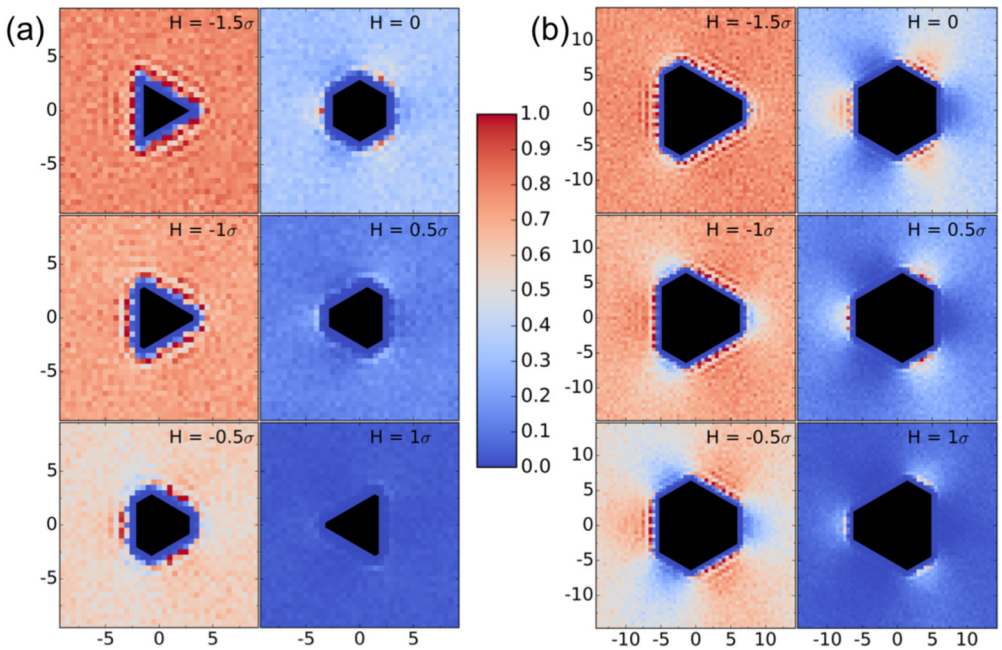

FIG. 2. Density profile of the bottom solvent (S2) when a cubic NP is fixed at the origin in the $\{111\}$ facet up orientation. Different images represent the density profiles at various vertical positions (unscaled). The black shaded region represents the area excluded by a perfect (not polybead) cubic NP from the vertical plane. The NP edge length is (a) 5σ and (b) 10σ. The color code is calibrated to the number density of beads of S2, ρ_{S2} such that the most red corresponds to the pure S2 phase and the most blue to the absence of S2 beads (i.e., pure S1 phase in the fluid region).

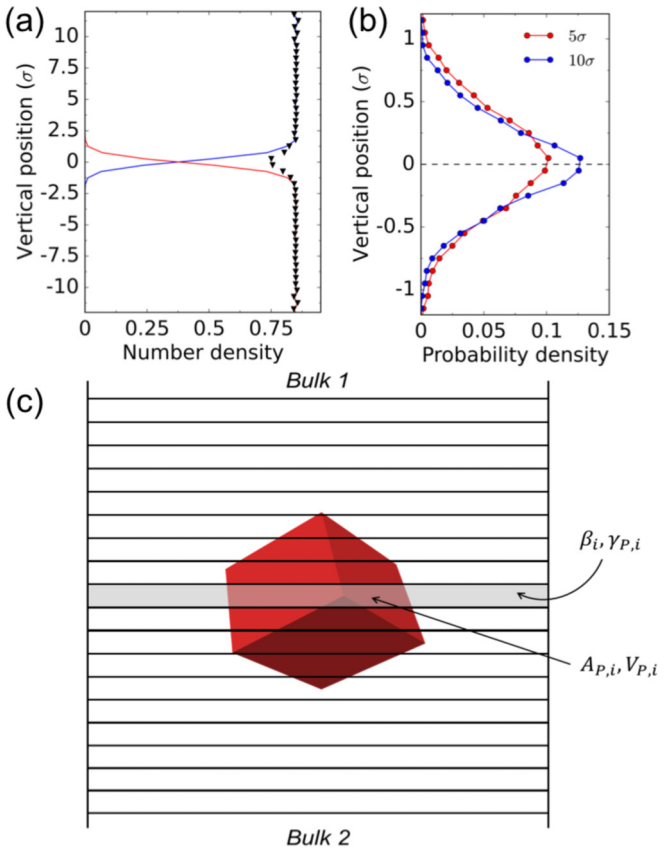

FIG. 3. Key properties of fluid-fluid interface. (a) Bead number densities ($1/\sigma^3$) of the bottom fluid (red), top fluid (blue), and combined fluid (black triangles). (b) Probability density (of center of mass) of an unconstrained polybead cube of size $e = 5\sigma$ (red) and 10σ (blue) at the interface. (c) Representation of the theoretical model describing the division of the system into vertical slabs.

play a significant role in determining the NP orientation at the interface. This increasing trend in capillary height with particle size is inconsistent with the size-independent prediction of $0.15e$ made by Soligno *et al.*, although such a theoretical value is in line with ours for the 10σ NP case. The likely cause for this deviation in behavior is the breakdown of the theoretical assumption of a sharp interface when the size of the NP is of the same order of magnitude as the size of the solvent molecules. In reality, the two fluids are not completely immiscible and they partially mix over a finite region [37].

To illustrate the significance of the finite-interface thickness, we simulated the two vertically stacked fluids and plotted the density of the fluid "beads" as a function of H in the absence of any NP [see Fig. 3(a)]. We note that, in this case, the contact angle is $\sim 90^\circ$ ($\varepsilon_{S1,S2} = 0.5$). The density of the bottom solvent, S2 (red curve) gradually decreases, while that of the top solvent, S1 (blue curve) gradually increases as we increase H over a small region from -1.5σ to 1.5σ. We henceforth refer to this region as the mixing region whose width is approximately 3σ. It is seen that the overall density of the fluid beads [black triangles in Fig. 3(a)] decreases in the mixing region. This low-density region arises from the unfavorable contact between the two types of fluid beads, which is captured by a low value of $\varepsilon_{S1,S2}(=0.5)$, and further leads to the low miscibility between the two fluids.

Note that the capillary deformation shown in Fig. 2 would be slightly smeared out if the NP's position and orientation were not fixed but allowed to fluctuate due to thermal (Brownian) motion. This is because by virtue of thermal energy, the vertical position (and orientation) of a small NP fluctuates significantly about the interface-dividing plane. Figure 3(b) shows the probability distribution of cubic NPs (of edge size, $e = 5\sigma$ and 10σ) as a function of vertical position where the standard deviation about the mean (the interface-dividing plane) for both sizes is approximately 0.35σ.

To account for NP behavior at these smaller length scales ($e = 5\sigma$), we propose an alternate theoretical model where we explicitly account for the contribution of the mixing region to the total energy of the system. We assume negligible contribution from capillary deformations, a simplification partially justified by the small length scales of interest. We divide the fluid system into a large number of adjacently placed, vertical slabs [Fig. 3(c)]. The total potential energy of the system is given as the sum of contributions by each slab. The function is shifted such that the energy of a NP completely immersed in the bulk of fluid 2 is zero:

$$\Delta F(H,\theta,\psi) = \sum_{i=\text{Bulk 1}}^{\text{Bulk 2}} (\gamma_{P,i} - \gamma_{P,\text{Bulk 2}}) A_{P,i} + (\beta_{\text{Bulk 2}} - \beta_i) V_{P,i}, \quad (4)$$

where $\gamma_{P,i}$ is the interfacial tension between the NP and the fluid phase in the slab, and β_i is the internal energy per unit volume of fluid phase in the slab. $A_{P,i}$ and $V_{P,i}$ represent the lateral surface area and the volume of NP in the slab, respectively. Since the interface (mixing region) is a region of unfavorable contact between immiscible solvents, the NP attempts to minimize the volume of the "unfavorable interfacial contact" by maximizing the volume it occupies inside the mixing region. Essentially, the variational principle of finding the values of H, θ, and ψ that minimize the system energy translates now to minimizing the volume of contact, as opposed to minimizing the planar area of contact. Further details on the minimization procedure are outlined in the Supplemental Material (SM, Sec. 2 [30]).

IV. RESULTS AND DISCUSSION

A. Single cubic particle at the interface

Figure 4(a) shows the underlying FE profile as a function of the vertical height, leaving the NP orientation unconstrained. It can be seen that a cube of edge size $e = 5\sigma$ pays a penalty of $\sim 10\, k_B T$ to move $\sim 0.3\, e$ away from the interface-dividing plane. It is clear from the underlying FE profile that the NP can only reside in a small region near the interface [Fig. 3(b)].

Figure 4(b) shows the FE landscape obtained from US calculations with θ and ψ as parameters (which probe all possible orientations of a cubic NP), while allowing the NP to freely fluctuate perpendicular to the interface. For this "base" case, the contact angle between the NP and both fluids was $\sim 90^\circ$ (i.e., $\varepsilon_{S1,NP} = \varepsilon_{S2,NP} = 0.5$) and $\varepsilon_{S1,S2}$ was set to 0.5. It is observed that the cubic NP exhibits the strongest preference for

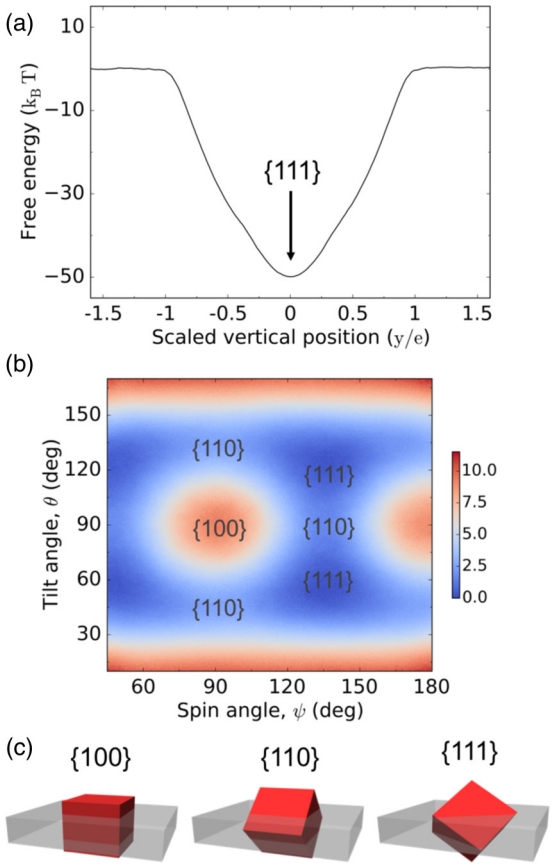

FIG. 4. (a) FE as a function of H for a polybead cube ($e = 5\sigma$) at base case conditions. The most preferred orientation is $\{111\}$ up near the interface-dividing plane. (b) Orientational FE landscape for cube ($e = 5\sigma$) marked with the locations of $\{100\}$, $\{110\}$, and $\{111\}$ up orientations (scale bar in k_BT units). (c) Depiction of the $\{100\}$, $\{110\}$, and $\{111\}$ up orientations of the cube, with the gray region representing the finite interfacial mixing region (for simplicity, the polybead cube is shown as a perfect cube).

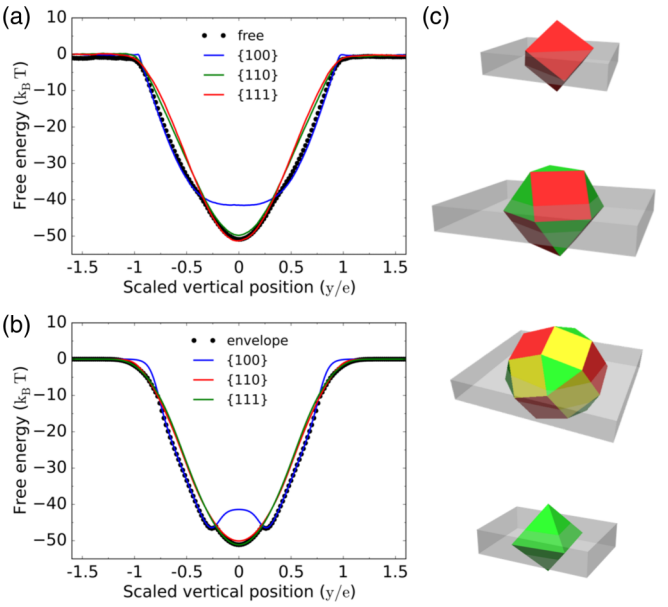

FIG. 5. FE vs H for a cube at the base conditions corresponding to three major orientations (blue, red, and green). (a) Polybead model with $e = 5\sigma$. The dotted black curve represents the unconstrained (or free-to-rotate) case [Fig. 4(a)]. (b) Continuum model. (c) Most preferred orientation for four studied polyhedral shapes at base conditions (from top to bottom): Cube: $\{111\}$, cuboctahedron: $\{111\}$, rhombicuboctahedron: $\{1n0\}$, octahedron: $\{100\}$.

the $\{111\}$ facet up configuration [see Fig. 4(c)], while it shows the smallest preference for the $\{100\}$ facet up configuration.

In general, it was observed that pinning the NP at different vertical positions (H) causes a change in its orientational preference. To probe this behavior, we break down the FE landscape, along the NP vertical position, into independent contributions from various orientational configurations. To do this, we fixed the orientation (θ and ψ) of the NP, and performed a one-dimensional (1D) US calculation (similar to that described in Sec. II B) with the vertical position as the only parameter. This procedure was repeated for three orientations, namely, $\{100\}$, $\{110\}$, and $\{111\}$ up [shown in Fig. 4(c)]. Figure 5(a) shows the FE profiles for a polybead cube of size 5σ with these fixed orientations and for the unconstrained case. It is observed that the unconstrained vertical FE landscape forms the lowermost envelope of all such possible curves corresponding to different orientations. For any vertical position, the orientation with the lowest free energy would be expected to be most stable. This implies that each point in said envelope corresponds to the most stable orientation (lowest FE) at that vertical position.

It can be seen [in Fig. 5(a)] that the FE of the $\{111\}$ facet up orientation is lower than that of both the $\{100\}$ and $\{110\}$ facet up orientations. The $\{100\}$ facet up configuration is stable beyond a certain distance ($\sim 0.4e$) from the interface-dividing plane. This $\{111\}$-up to $\{100\}$-up change in preferential orientation is characterized by a slight flattening of the FE profile, followed by a change in its slope. These characteristics are correctly predicted by our version of the continuum model as seen in Fig. 5(b). The parameters needed in the model are calculated by fitting the MD simulation results to Eq. (4) (details given in the SM, Sec. 2 [30]).

The US approach to find the most preferred orientation of NPs can be applied to different polyhedral shapes. We present results for four different NP shapes in Fig. 5(c) of similar sizes, with additional details given in the SM, Sec. 5 [30].

B. Tuning orientation preference of NP by changing relative contact angles

For practical applications, it is important to understand how the interfacial properties of the fluids and the NP affect the preferential orientation that an isolated NP will exhibit at the fluid-fluid interface. We show here how such different NP orientations can be accessed and favored, by tuning the relative inter-species interaction parameters. In particular, we consider two cases:

(1) Changing $\varepsilon_{S1,S2}$—the degree of miscibility between the two solvents: Increasing $\varepsilon_{S1,S2}$ increases the miscibility of the two fluids and, to some degree, leads to an increase in the width of the mixing region. For a higher value of $\varepsilon_{S1,S2}$, we observed a relatively shallower free-energy profile

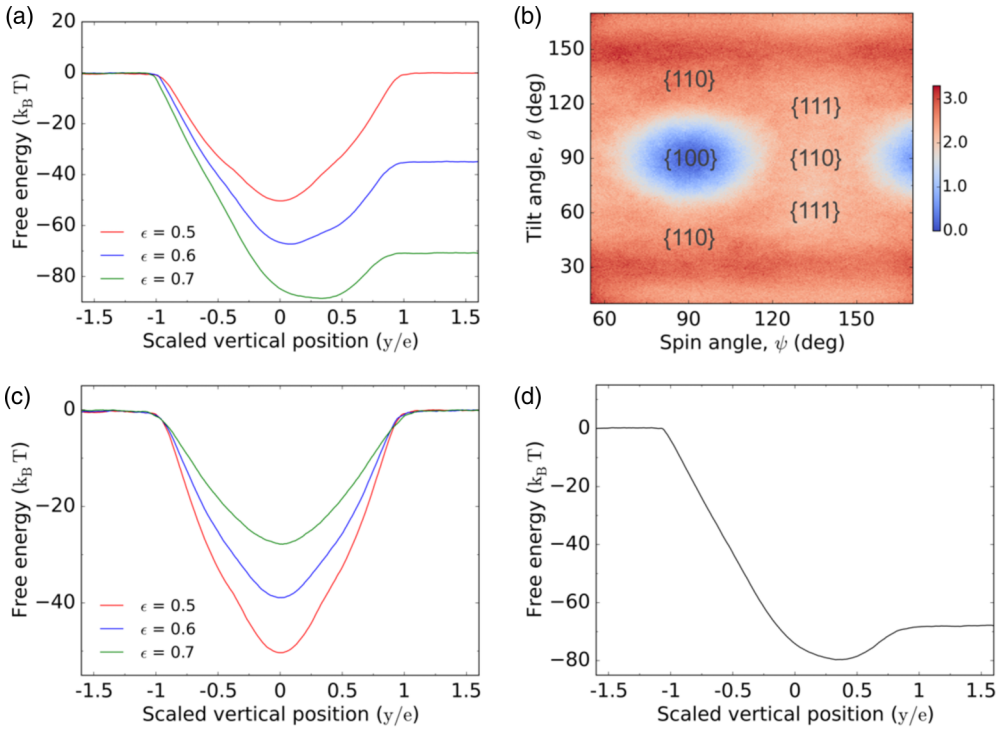

FIG. 6. FE characteristics for a cube of edge 5σ; (a) FE vs H for different values of $\varepsilon_{\mathrm{NP,S1}}$ keeping $\varepsilon_{\mathrm{S1,S2}}(=0.5)$ fixed. (b) Orientational FE landscape marked with the locations of $\{100\}$, $\{110\}$, and $\{111\}$-up orientations with $\varepsilon_{\mathrm{NP,S1}} = 0.7$ and $\varepsilon_{\mathrm{S1,S2}} = 0.5$. (c) FE vs H for different values of $\varepsilon_{\mathrm{S1,S2}}$ keeping $\varepsilon_{\mathrm{NP,S1}} = \varepsilon_{\mathrm{NP,S2}} = 0.5$ fixed. Higher values of $\varepsilon_{\mathrm{S1,S2}}$ generate successively shallower wells. (d) FE vs H with $\varepsilon_{\mathrm{S1,S2}} = 0.6$, $\varepsilon_{\mathrm{NP,S1}} = 0.7$; the cube's most preferred position shifts upwards to $\sim 0.3e$, and its most preferred orientation changes from $\{111\}$ to $\{100\}$ facet up.

[Fig. 6(c)] along the vertical position. This result is consistent with the predictions from the continuum model since if the fluids are more miscible, the energy per unit volume (β_i) in the mixing region is relatively lower. As per Eq. (4), a smaller negative value of the prefactor ($\beta_{\mathrm{Bulk}\,2} - \beta_i$) for the excluded volume term ($V_{P,i}$) will give a shallower FE profile. A shallower FE well allows the NP to symmetrically access higher vertical positions by virtue of its thermal energy.

(2) Changing $\theta_{\mathrm{NP,S}}$—the contact angles between solvents and the NP: By decreasing $\theta_{\mathrm{NP,S1}}$ (i.e., increasing $\varepsilon_{\mathrm{NP,S1}}$), we give the NP an enthalpic preference to solvent 1 relative to solvent 2. The NP now prefers to be solvated by solvent 1 and thus has an incentive to move away from the interface-dividing plane. As shown in Fig. 6(a), this change expectedly shifts the global minimum of the vertical FE profile to a higher $H = H^*$, effectively changing the NP's mean position from 0.0 to H^*. From the continuum perspective, due to the lower energy of interactions between NP and fluid 1, fluid slabs with a higher concentration of fluid 1 have a lower value of $\gamma_{P,i}$. Thus, the FE in the bulk of fluid 1 is lower than that in the bulk of fluid 2.

As discussed before (for the symmetric case in Sec. IV A), there exists a strong correlation between the NP's vertical position and preferred orientation. Thus, by altering the NP's mean vertical position through changes in $\theta_{\mathrm{NP,S1}}$, we can indirectly change its orientation behavior. This is shown in Fig. 6(b), where for $\varepsilon_{\mathrm{NP,S1}} = 0.7$ we see a change in the preferred orientation of the NP from $\{111\}$ to $\{100\}$. We, however, also see that the depth of the orientational bias well is small ($\sim 3k_BT$). This is the result of the effective flattening of the vertical FE profile over a large range of positive H values [Fig. 6(a), green curve] for $\varepsilon_{\mathrm{NP,S1}} = 0.7$. In such a situation, the NP can reside over a wide range of H with almost equal probability, while accessing different orientations at different H. So, in this case a reduction in positional selectivity leads to a corresponding reduction in orientational selectivity.

If maintaining orientational selectivity is important, an alternative approach to tune NP orientation involves modifying both $\varepsilon_{\mathrm{S1,S2}}$ and $\theta_{\mathrm{S1,NP}}$ synergistically to gain a finer control over the shape of the FE profile. We can see from Fig. 6(d) that for $\varepsilon_{\mathrm{S1,NP}} = 0.7$ and $\varepsilon_{\mathrm{S1,S2}} = 0.6$ for a cube of 5σ size, the FE minimum is shifted from $H = 0.0$ to $H = 1.5\sigma$, without flattening the profile. In this manner, we retain the positional selectivity while accessing a different preferential NP orientation (namely, $\{100\}$ facet up).

C. Assembly of two particles at the interface

Towards a future goal of describing multi-NP interfacial assembly, we attempt here to explain two-NP behavior at the interface as an extension to the insights on single-NP behavior described in Secs. IV A and IV B. As it will be shown, two-NP interfacial assembly can be explained by the interplay of the underlying FE characteristics for individual NPs at the interface and the FE associated with NP-NP interactions. For this purpose, we illustrate our analysis using cuboctahedra (CO) whose NP-NP interactions are richer than those of cubes given that the former can contact each other through two

different types of facets. Also, to model NP-NP interactions, we need to specify the interaction parameter $\varepsilon_{NP,NP}$ between two Lennard-Jones beads belonging to the two different NPs (details in SM, Fig. S7 [30]). By synergistically selecting appropriate values of $\varepsilon_{NP,NP}$ and $\varepsilon_{NP,S1}$, one can potentially calibrate the inter-NP attraction to mimic experimental behavior.

As dictated by its FE characteristics (see Fig. S4 in SM [30]), for the base case (i.e., $\varepsilon_{S1,NP} = \varepsilon_{S2,NP} = \varepsilon_{S1,S2} = 0.5$) an isolated CO prefers to stay close to the interface-dividing plane while orienting with its $\{111\}$ facet up. However, as soon as two cuboctahedra join at the square $\{100\}$ facet, an additional constraint is added to the system. Now, it is geometrically impossible for both COs to individually satisfy all three (positional, orientational, contact) constraints simultaneously. If we assume a situation wherein the inter-NP attraction is strong enough to force a complete (square-square) contact constraint (e.g., for $\varepsilon_{NP,NP} \geqslant 0.15$), the system now faces the following choices:

(1) If the COs remain close to the interface-dividing plane, they can either orient with their $\{100\}$ facets up to form a square motif or they can orient with their $\{110\}$ facets up to form a linear rodlike motif. In both of these situations, the COs pay an orientational FE penalty ($\sim 10\,k_BT$ per CO), or

(2) If the COs attempt to orient in the desired $\{111\}$ facet up orientation, a vertical distance separates their centers, as seen in Fig. 7(a). In this case, they pay a penalty ($\sim 15\,k_BT$ per CO) for moving up in the positional FE well (Fig. S4 in SM [30]). Moreover, if the particles move too far away from the interface-dividing plane, their orientation preference changes from $\{111\}$ facet up to $\{110\}$ facet up.

Depending on the specific values of the parameters characterizing the NP-NP and NP-fluid interactions ($\theta_{NP,S}$, size of the CO, etc.), the system finds a preferred configuration that constitutes a compromise between the competing constraints. For $e = 5\sigma$, the order of magnitude of positional and orientational FE penalties (as measured from the minimum value) is comparable, so the system spontaneously chooses a state intermediate between states (1) and (2) as shown in Fig. 7(c).

By setting the inter-NP attraction to a relatively low value (e.g., $\varepsilon_{NP,NP} = 0.125$), it is possible to relax the strong contact constraint. In such a scenario, the NPs forgo the energetic advantage of a complete (square-square) contact, and slip along the contact surface. In doing so, the NPs reduce the vertical separation between their centers and, as a result, come closer to the interface-dividing plane. This structure [shown in Figs. 7(b) and 7(d)] is the basic motif in the superstructure referred to as the puckered honeycomb structure.

The strategy developed for modifying the FE for a single NP (Sec. IV B) can be extended to a two-NP system as follows. For the purpose of stabilizing the puckered honeycomb motif, the degree of miscibility between the two fluids ($\varepsilon_{S1,S2}$) can be increased (without changing the relative contact angles of the fluids with the CO). By doing this, the FE well associated with the vertical position becomes shallower, thereby allowing the CO to access a wider range of vertical positions around the interface-dividing plane (as shown in Sec. IV B). Similarly, we can reduce the contact angle between the NP and the top fluid, $\theta_{NP,S1}$ (corresponding to $\varepsilon_{NP,S1} = 0.7$) such that the most preferred position is centered about 1.5σ–2.0σ [Fig. 7(e)]. At this vertical position, the COs preferentially orient themselves with the $\{110\}$ facet up configuration, with no significant relative separation distance between NP centers. This gives rise to stable linear, rodlike structures [Fig. 7(f)]. It is important to note that if $\varepsilon_{NP,S1}$ is increased, $\varepsilon_{NP,NP}$ has to be readjusted to mitigate the NP's solvation preference to fluid S1; specifically, if $\varepsilon_{NP,S1}$ is set to 0.7, then $\varepsilon_{NP,NP}$ must be increased from 0.125 to ~ 0.25.

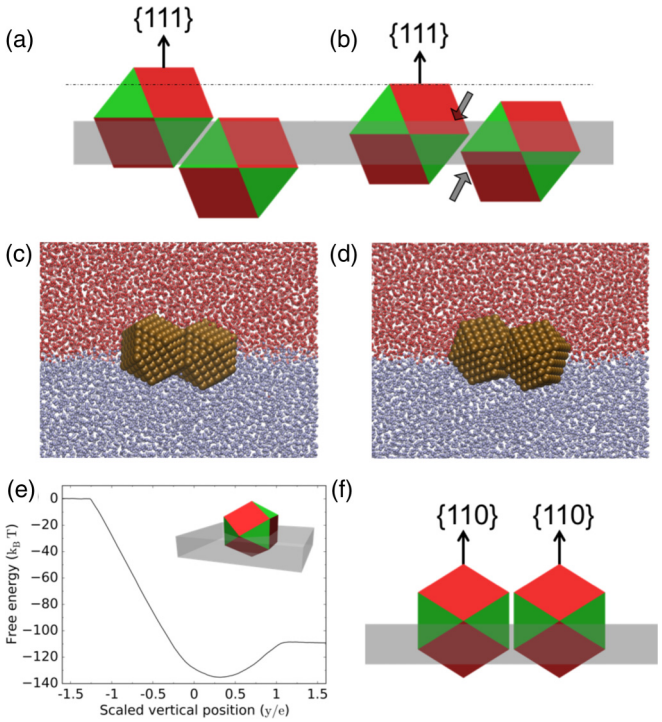

FIG. 7. (a,b) are cartoon representations of two COs at the interface (gray region) with their $\{111\}$ facets pointing vertically upwards. In (a) the contact between the square faces of the COs is complete, causing the COs to move away from the interface-dividing plane and out of the interface, hence decreasing the system's stability. In (b) the COs can slip along their contacting surface and move into the interface, reducing, in the process, the vertical separation between their centers of mass. (c) Snapshot from brute-force MD simulation of two COs with $e = 5\sigma$ and $\varepsilon_{NP,NP} = 0.15$. The complete contact constraint (due to high $\varepsilon_{NP,NP}$ value) forces the joined structure to rotate as a whole, thereby bringing the NP centers closer to the interface-dividing plane. The solvent beads are represented as small dots for better visibility. (d) $e = 5\sigma$, $\varepsilon_{S1,S2} = 0.7$, and $\varepsilon_{NP,NP} = 0.125$. The COs eventually attain and retain this structure even when initialized far away. (e) FE profile for a CO ($e = 5\sigma$) and $\varepsilon_{NP,S1} = 0.7$. Under these conditions, CO prefers to stay at $H \sim 0.4e$ and with its $\{110\}$ facet up. (f) Stable rodlike motif formed by two COs. The interfacial region in the snapshots is shown in gray.

D. Validity of the continuum model

As can be seen in Fig. 5(b), the continuum model proposed in Sec. III is able to capture semiquantitatively the key features and trends of behavior of the FE plots for the polybead, solvent-explicit model and associated orientational and positional preferences of a single NP at a fluid-fluid interface. Compared to the sharp-interface model [24], the continuum model that we propose here gives a more detailed description of the system

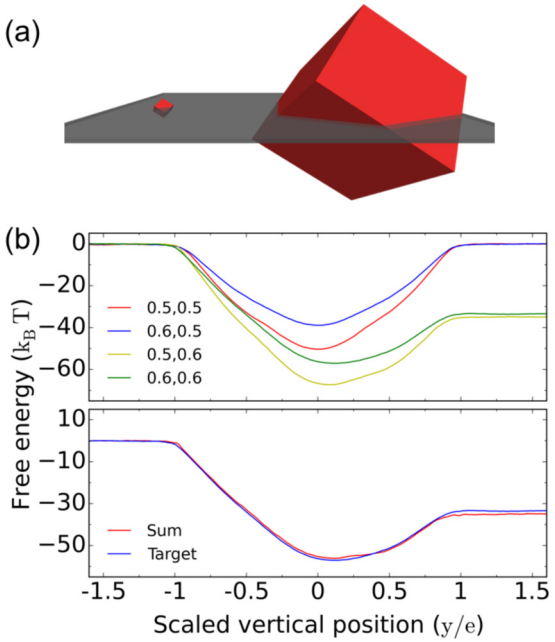

FIG. 8. (a) Illustration of the idea that if the NP size is much bigger than the characteristic thickness of the interface (as in the rightmost cube), the proposed finite-interface model approaches the sharp-interface model. (b) (Top) MD simulation results for a polybead cube ($e = 5\sigma$) for different sets of ($\varepsilon_{S1,S2}$,$\varepsilon_{NP,S1}$) parameter values. (Bottom) The sum (red curve) of changes in FE (ΔF) caused by independent changes in parameters to the base FE profile matches with the profile generated by changing both parameters simultaneously (target function, blue curve).

when the size of the NP is within the same order of magnitude as the size of the liquid molecules. An elegant feature of this formulation lies in the fact that it reduces to the previous sharp-interface model in the limit of very large NP sizes, as illustrated in Fig. 8(a). Indeed, when the size of the NP is much greater than the width of the interface, we can write

$$\text{Excluded volume}(V_{ex}) \approx (\text{Excluded area} \times \text{interface width}),$$

$$\text{NP area in contact with the mixing region} \approx (\text{Perimeter} \times \text{interface width}).$$

As we saw in Sec. IV A, this continuum model correctly predicts the positional FE minimum for a cube. As further validation, we generated FE vs H profiles, for a single cube ($e = 5\sigma$) at the interface, for different sets of ($\varepsilon_{S1,S2}$,$\varepsilon_{NP,S1}$) values [Fig. 8(b), top panel]. Each profile is labeled using the $F(\varepsilon_{S1,S2},\varepsilon_{NP,S1})$ notation. Next, we calculated the change in the FE (ΔF) (at corresponding values of H) caused by a change in one parameter at a time. We, then, added the change caused by both parameters individually to the base value [F(0.5,0.5)]. It can be seen in the bottom panel of Fig. 8(b) that this sum is equal to the target function [F(0.6,0.6)]. This additivity of individual FE effects for the solvent-explicit polybead model agrees with the linear structure of the relevant terms in the continuum model formulation [Eq. (4)] (nonlinear effects are absent):

$$F(0.5, 0.5) + [F(0.6, 0.5) - F(0.5, 0.5)] + [F(0.5, 0.6) - F(0.5, 0.5)] = F(0.6, 0.6), \quad (5)$$

or,

$$F_{\text{base}} + \Delta F(\varepsilon_{S1,S2}) + \Delta F(\varepsilon_{NP,S1}) = F_{\text{target}}. \quad (6)$$

V. CONCLUSIONS

By using a polybead model, we simulated an isolated NP at an explicitly defined fluid-fluid interface. Using biased sampling techniques, we mapped the orientational and positional FE function for a cubic NP. In general, this methodology can be applied to any polyhedral shape (as illustrated in the SM, Sec. 5 [30]), provided it can be formed using a polybead model. We found that an isolated cube at the interface, with no selective preference to either fluids, prefers a {111} up orientation. A Pieranski-type formulation [22] of the continuum model presented in Refs. [23,24], however, predicts a {110} up orientation. It was found that when the width of the mixing region is not negligible relative to the size of the cube, the effect of this finite interface on the underlying FE is significant. The FE trends observed in the MD simulations were justified based on the proposed finite-interface-thickness continuum model. This model enacts the principle of minimization of interfacial energy based on reducing the interfacial volume (i.e., the volume of the mixing region) by maximizing the volume occupied therein by the NP.

Thereafter, we proposed a strategy to gain access to different orientational configurations for a given NP shape. By changing the contact angles between the three system components, we can alter the shape and depth of the FE wells (that govern both positional and orientational behavior) to create conditions at which different target configurations of the NP can be stabilized. We showed that for certain conditions ($\varepsilon_{S1,S2} = 0.6, \varepsilon_{NP,S1} = 0.7$) a cube of edge size $e = 5\sigma$ moves away from the interface-dividing plane and orients with its {100} facet up. We then built upon these principles to explain and control the assembly of two COs. Indeed, we predicted conditions for the stability of different types of assemblies and validated our predictions through direct MD simulations.

We expect that the approaches developed in this study and the results generated therefrom to be potentially translatable to real systems and guide experimental efforts to improve protocols for interfacial assembly of NPs. Although, specific NP materials and fluids can be approximately mapped into our coarse-grained model by calibrating the different contact angles between the solid and fluid phases, several refinements can be introduced. For example, the NP model can be more detailed by using more numerous beads to represent its surface. We could even introduce facet-specific interactions (patchy NPs) by setting different $\varepsilon_{NP,S}$ values for beads belonging to different types of facets. This would be of interest for certain kinds of NP shapes like cuboctahedra or rhombicuboctahedra. Alternatively, this could also be achieved by adding grafted ligands onto the NP beads [38] (if existing in the real system).

Likewise, more atomistic models could be used to describe specific solvents [39].

The implicit-solvent continuum model we propose and validate is also expected to be a valuable tool to model the interfacial behavior of NPs in the regime where the NP size is of the same order of magnitude as the solvent size or the interface thickness. For small NPs, we conjecture that the dynamic nature of the NP motions (both translation and rotation) perpendicular to the interface tends to average the capillary deformations into an effective mixing region. Through application of this analytical model, one can gain a more complete and intuitive understanding of the underlying physics that govern the relative stability of different NP orientations at various vertical positions. There exist different directions that can be pursued to improve the theory. For example, a more detailed model could be developed by further decoupling the effect of the deformation of the diving surface in contact with the NP from the average width of the mixing region. In this context, simulations of NPs of increasingly larger sizes (relative to the interface thickness) will also be informative to detect and quantify the contributions of capillary deformations and interfacial mixing.

Future modeling studies could extend our work by probing the effect of NP solvent wetting at a vapor-liquid interface instead of a liquid-liquid interface. Also, multiparticle interfacial assembly behavior can be studied by using solvent-explicit coarse-grained models or be aided by a solvent-implicit continuum model like those presented here. Work along these lines is currently under way.

ACKNOWLEDGMENTS

The authors acknowledge funding support from a SEED Grant provided by a National Science Foundation (NSF) MRSEC award to Cornell, Grant No. DMR-1120296, and from NSF Award No. CBET-1402117. The authors are also grateful to Dr. Vikram Thapar and Professor Paul H. Steen for useful exchanges. This work used the Extreme Science and Engineering Discovery Environment (XSEDE), which is supported by NSF Grant No. ACI-1053575.

[1] W. J. Baumgardner, K. Whitham, and T. Hanrath, Nano Lett. **13**, 3225 (2013).
[2] W. H. Evers, B. Goris, S. Bals, M. Casavola, J. de Graaf, R. V. Roij, M. Dijkstra, and D. Vanmaekelbergh, Nano Lett. **13**, 2317 (2013).
[3] S. Dasgupta, M. Katava, M. Faraj, T. Auth, and G. Gompper, Langmuir **30**, 11873 (2014).
[4] W. van der Stam, A. P. Gantapara, Q. A. Akkerman, G. Soligno, J. D. Meeldijk, R. van Roij, M. Dijkstra, and C. de Mello Donega, Nano Lett. **14**, 1032 (2014).
[5] E. Kalesaki, W. H. Evers, G. Allan, D. Vanmaekelbergh, and C. Delerue, Phys. Rev. B **88**, 115431 (2013).
[6] P. O. Anikeeva, J. E. Halpert, M. G. Bawendi, and V. Bulović, Nano Lett. **9**, 2532 (2009).
[7] P.-P. Fang, S. Chen, H. Deng, M. D. Scanlon, F. Gumy, H. J. Lee, D. Momotenko, V. Amstutz, F. Cortés-Salazar, C. M. Pereira, Z. Yang, and H. H. Girault, ACS Nano **7**, 9241 (2013).
[8] L Mangolini, A. E Thimsen, and U. Kortshagen, Nano Lett. **5**, 655 (2005).
[9] J. Baxter, Z. Bian, G. Chen, D. Danielson, M. S. Dresselhaus, A. G. Fedorov, T. S. Fisher, C. W. Jones, E. Maginn, U. Kortshagen, A. Manthiram, A. Nozik, D. R. Rolison, T. Sands, L. Shi, D. Sholl, and Y. Wu, Energy Environ. Sci. **2**, 559 (2009).
[10] A. J. Nozik, M. C. Beard, J. M. Luther, M. Law, R. J. Ellingson, and J. C. Johnson, Chem. Rev. **110**, 6873 (2010).
[11] D. V. Talapin, J.-S. Lee, M. V. Kovalenko, and E. V. Shevchenko, Chem. Rev. **110**, 389 (2010).
[12] Z.-Y. Zhou, N. Tian, J.-T. Li, I. Broadwell, and S.-G. Sun, Chem. Soc. Rev. **40**, 4167 (2011).
[13] G. W. Crabtree and J. L. Sarrao, MRS Bull. **37**, 1079 (2012).
[14] U. Agarwal and F. A. Escobedo, Nat. Mater. **10**, 230 (2011).
[15] P. F. Damasceno, M. Engel, and S. C. Glotzer, Science **337**, 453 (2012).
[16] V. Thapar, T. Hanrath, and F. A. Escobedo, Soft Matter **11**, 1481 (2015).
[17] A. P. Gantapara, J. de Graaf, R. van Roij, and M. Dijkstra, Phys. Rev. Lett. **111**, 015501 (2013).
[18] S. Razavi, J. Koplik, and I. Kretzschmar, Soft Matter **9**, 4585 (2013).
[19] H.-M. Gao, Z.-Y. Lu, H. Liu, Z.-Y. Sun, and L.-J. An, J. Chem. Phys. **141**, 134907 (2014).
[20] W. Ramsden, Proc. R. Soc. London **72**, 156 (1903).
[21] S. U. Pickering, J. Chem. Soc., Trans. **91**, 2001 (1907).
[22] P. Pieranski, Phys. Rev. Lett. **45**, 569 (1980).
[23] J. de Graaf, M. Dijkstra, and R. van Roij, Phys. Rev. E **80**, 051405 (2009).
[24] J. de Graaf, M. Dijkstra, and R. van Roij, J. Chem. Phys. **132**, 164902 (2010).
[25] G. Soligno, M. Dijkstra, and R. van Roij, Phys. Rev. Lett. **116**, 258001 (2016).
[26] G. Morris, S. J. Neethling, and J. J. Cilliers, Miner. Eng. **23**, 979 (2010).
[27] G. Morris, S. J. Neethling, and J. J. Cilliers, Miner. Eng. **33**, 87 (2012).
[28] J. J. Choi, K. Bian, W. J. Baumgardner, D.-M. Smilgies, and T. Hanrath, Nano Lett. **12**, 4791 (2012).
[29] M. P. Boneschanscher, W. H. Evers, J. J. Geuchies, T. Altantzis, B. Goris, F. T. Rabouw, S. A. P. van Rossum, H. S. J. van der Zant, L. D. A. Siebbeles, G. Van Tendeloo, I. Swart, J. Hilhorst, A. V. Petukhov, S. Bals, and D. Vanmaekelbergh, Science **344**, 1377 (2014).
[30] See Supplemental Material at http://link.aps.org/supplemental/10.1103/PhysRevMaterials.1.055602 for details of the simulation methodology and the proposed continuum model, and for additional FE results for different particle shapes.
[31] M. R. Khadilkar and F. A. Escobedo, J. Chem. Phys. **137**, 194907 (2012).
[32] S. Plimpton, J. Comput. Phys. **117**, 1 (1995).
[33] D. Duque, J. C. Pàmies, and L. F. Vega, J. Chem. Phys. **121**, 11395 (2004).

[34] E. S. Savoy and F. A. Escobedo, Langmuir **28**, 3412 (2012).
[35] G. M. Torrie and J. P. Valleau, J. Comput. Phys. **23**, 187 (1977).
[36] S. Kumar, J. M. Rosenberg, D. Bouzida, R. H. Swendsen, and P. A. Kollman, J. Comput. Chem. **13**, 1011 (1992).
[37] M. Meyer, M. Mareschal, and M. Hayoun, J. Chem. Phys. **89**, 1067 (1988).
[38] S. Goyal and F. A. Escobedo, J. Chem. Phys. **135**, 184902 (2011).
[39] A. P. Kaushik and P. Clancy, J. Comput. Chem. **34**, 523 (2013).